JOURNAL OF GEOPHYSICAL RESEARCH, VOL. 93, NO. A8, PAGES 8602-8612, AUGUST 1, 1988

Analytic Formulation and Quantitative Solutions of the Coupled ULF Wave Problem

XIAOMING ZHU AND MARGARET G. KIVELSON

Department of Earth and Space Sciences and Institute of Geophysics and Planetary Physics University of California at Los Angeles

In the terrestrial magnetosphere, the inhomogeneous magnetic field and plasma density give rise to a continuous spectrum of field line resonant frequencies. Compressional disturbances with characteristic frequencies lying within the range of the spectrum may couple to transverse oscillations of resonant field lines. The coupling is of particular interest for global compressional modes trapped in the magnetic cavity. These modes decay in time through the coupling, even in the absence of dissipation. The importance of the process is that, through the damping of the global modes, large-scale motion can drive localized field line resonances. In this study, we investigate the mode coupling and examine the parameter dependence of the damping rate of the global mode. The problem is discussed as an initial value problem in the box model which retains most of the significant physics yet remains mathematically tractable. To treat the coupling, we use the analogy of Landau damping in a homogeneous plasma. From the Laplace transform approach, we obtain the complex frequencies of the compressional wave by finding the singularities of the associated Green's function. Once the complex frequency has been found numerically, we obtain the corresponding waveforms in the box. Many observed wave properties can then be obtained. The calculations agree well with other simulation work and correspond to results obtained for the reflection of radio waves from the ionosphere and for plasma heating by absorption of radiation.

INTRODUCTION

Ultralow frequency (ULF) waves are magnetohydrodynamic waves present in the terrestrial magnetosphere [*Cummings et al.*, 1969; *Samson*, 1972]. Extensive theoretical and observational efforts have been made during the past decades in order to understand the phenomenon (see the review paper by *Southwood and Hughes*, [1983] and the references therein). Observed ULF perturbations have been classified into two types: continuous pulsations (Pc) and irregular pulsations (Pi). Both types have been further subdivided by their periods. For the continuous pulsations, the Pc 3, Pc 4 and Pc 5 period bands are 10–45 s, 45–150 s and 150–600 s, respectively [Jacobs et al., 1964]. For Pc 3–5 pulsations, the wavelength is of the order of a few R_e where R_e is the Earth's radius [*Southwood and Hughes*, 1983]. Thus these types of pulsations arise from large-scale perturbations of the magnetospheric system. They are predominantly dayside phenomena that fall into two classes. In one class, the pulsations are harmonically structured and azimuthally polarized. The fundamental pulsation frequency varies with local time and radial distance, and the spectrum is dominated by resonances of local magnetic field lines [*Takahashi and McPherron*, 1982; *Engebretson et al.*, 1986]. In the other class, the perturbation has a substantial compressional component and a large part of the magnetosphere oscillates at a single perturbation frequency [*Kivelson et al.*, 1984; *Greenstadt et al.*, 1986]. As will be seen, both of these features are contained in the theory.

For theoretical modeling of the Pc 3–5 waves, the inhomogeneity of the system on a characteristic scale of a few R_e cannot be neglected. Inhomogeneity leads to a continuous spectrum of field line resonant frequencies, i.e., the resonant frequency changes continuously with radial distance. Consequently, a perturbation whose characteristic frequency lies within the range of the continuous spectrum may couple to a transverse oscillation of an appropriate field line (resonant field line). The mathematical complexity arising from the wave mode coupling prevents one from obtaining an analytic solution of the problem even in a dipole geometry [*Dungey*, 1967; *Cummings et al.*, 1969]. Nonetheless, early theoretical work on Pc 3–5 waves successfully described the ULF wave response to sources at the boundary of the magnetosphere [*Southwood*, 1974, 1975; *Chen and Hasegawa*, 1974*a*,*b*]. The sources are generally assumed to be the Kelvin-Helmholtz instabilities excited by the solar wind interaction with the magnetosphere. The theory of field line resonance explains how the perturbation energy of a monochromatic compressional wave couples to and excites the standing shear Alfvén mode on the resonant field line. The nature of the Kelvin-Helmholtz source requires large azimuthal wave numbers of the perturbation [*Chen and Hasegawa*, 1974*a*]. With this requirement, the ULF wave varies rapidly in phase across the field line in the azimuthal direction and has almost no phase variation in the radial direction, taken as the direction of plasma and field inhomogeneity. The field line resonance theory explains successfully the typical features of those ULF waves that are harmonically structured and azimuthally polarized and is, therefore, widely accepted.

Following the proposals of *Kivelson and Southwood* [1985], recent theoretical studies of ULF waves have considered the possibility of impulsive excitation of ULF waves in the magnetosphere [*Kivelson and Southwood*, 1985, 1986; *Allan et al.*, 1985, 1986*a*,*b*; *Inhester*, 1987].

Paper number 7A8926.
0148-0227/88/007A-8926$05.00

This theory (which will be referred to as the global mode theory) considers perturbations excited in the magnetosphere by an impulsive perturbation of the boundary as the system relaxes from its initial state. As its name suggests, the global mode theory identifies damped collective modes of the system that represent the response to an impulse. The physics of the modes is closely associated with that of the surface mode found by *Chen and Hasegawa* [1974*b*]. Chen and Hasegawa assumed a large azimuthal wave number, but in the global mode theory a comparatively smaller azimuthal wave number is assumed to account for certain features of the large-scale compression of the magnetosphere. Numerical simulations have confirmed the existence of the wave modes [*Allan et al.*, 1985, 1986*a,b*). Because previous work on the damped collective modes is basically either qualitative [*Kivelson and Southwood*, 1985, 1986] or lacks substantial analytical discussion [*Allan et al.*, 1985, 1986 *a,b*], the primary interest in the present work is to formulate more quantitative results and to unify the theory of field line resonance and the global mode theory. The problem is discussed in the box model which was first suggested by *Radoski* [1971]. We are aware that the simplified model differs in many respects from the real terrestrial magnetosphere; consequently it cannot explain all observational features, such as the absence of wave perturbations on the nightside of the magnetosphere. The analytical and numerical results can, however, provide insight into the wave coupling problem and can provide a step toward fully understanding ULF waves in a realistic model.

Mathematically, wave mode coupling in an inhomogeneous system is often represented by singular integral or differential equations. A well-known example of the singular integral equation arises for the electrostatic oscillation in a hot plasma. A singular integration appears in the dispersion relation of the perturbation. Landau recognized that the singularity arises from the interaction between the wave field and the so-called resonant particles whose velocities approximately match the wave phase velocity. Furthermore, Landau was able to show that the interaction could cause damping of the electrostatic wave perturbation with wave energy going into acceleration of the resonant particles for appropriate particle distributions. We will find that his approach is relevant to the problem we are going to solve.

In our problem, the inhomogeneity is in coordinate space and we start from a singular differential equation. The singularity occurs at the position of the resonant field line. Similar types of singular differential equations are encountered in other scientific disciplines. In hydrodynamics, the so-called critical layer problem has long been of interest. In stratified shear flow, the critical layer corresponds to the level where the mean flow velocity matches the perturbation wave velocity [*Lin*, 1955]. In ionospheric physics, attention has been directed to the reflection of radio waves from a stratified ionosphere; the signal is absorbed at a critical height where the radio wave frequency matches the local plasma frequency provided the wave electric field is polarized in the plane of incidence [*Budden*, 1961]. In fusion machines, electromagnetic waves are often used to heat plasma. The fundamental physics is almost identical to Budden's problem [*Appert et al.*, 1984]. Analytic and numerical calculations demonstrate that there exists an optimal incident angle for absorption of the incident radio waves by the plasma [*Piliya*, 1966; *White and Chen*, 1974; *Forslund et al.*, 1975; *Appert et al.*, 1984]. Because the physics is similar in these seemingly different subjects, the analysis and the numerical method discussed in this work should apply to related problems.

THE INHOMOGENEOUS BOX MODEL

To obtain quantitative results, a simplified model of the terrestrial magnetosphere is called for and we adopt *Radoski's* [1971] box model for our analysis. The model retains the essential coupling features of the magnetosphere but remains mathematically tractable. The cold plasma in this model is contained in a rectangular box embedded in a uniform magnetic field, B. The plasma is inhomogeneous in only one direction which defines the x axis. The magnetic field lines, perpendicular to the direction of the inhomogeneity, are along the z direction. The y axis completes the triad.

The boundary conditions of the problem must be considered. In the z direction, ionospheres anchor the field lines so that two boundaries can be placed at $z=\pm l$. The ionosphere is considered as a perfect reflector which leads to quantization of the wave number along the z direction. The variation in the azimuthal coordinate of an azimuthally symmetric magnetosphere can be represented by requiring all variables in the y direction to be periodic. The boundaries at large and small x correspond to the magnetopause and the plasmapause or equatorial ionosphere, respectively. At the magnetopause, the sudden jump of the plasma density and magnetic field produces a jump of the Alfvén velocity; conservation of Poynting flux implies that electric field signals, E, must decrease when the Alfvén velocity decreases as is the case outside of the magnetopause. Approximating the small electric field of the magnetosheath as a zero field and recognizing that the tangential electric field is continuous across the magnetopause, one can take a fixed boundary condition for the plasma displacement normal to the magnetopause. For the boundary condition in the inner magnetosphere, one may note that the lower boundary is located to the left of the turning point of the differential equation (see, e.g., (4) below) for representative magnetospheric parameters. Any solution to the left of the turning point either grows or decays exponentially. For a wave mode that has a reasonable wave amplitude in the whole spatial region, one has to take the decaying solution and the inner boundary condition can be taken again as a fixed boundary condition.

The differential equations for the MHD perturbations of a cold plasma are

$$\frac{\partial B}{\partial t} = \nabla\times(u\times B) \qquad \rho\frac{\partial u}{\partial t} = J\times B \qquad J = \nabla\times B/\mu_o \tag{1}$$

In the box model the above equations can be linearized and written as:

$$\left[\frac{1}{A^2}\frac{\partial^2}{\partial t^2} - \frac{\partial^2}{\partial z^2}\right]\xi_x = -\frac{1}{B}\frac{\partial b_z}{\partial x}$$

$$\left[\frac{1}{A^2}\frac{\partial^2}{\partial t^2} - \frac{\partial^2}{\partial z^2}\right]\xi_y = -\frac{1}{B}\frac{\partial b_z}{\partial y}$$

$$b_x = B\frac{\partial \xi_x}{\partial z} \qquad (2)$$

$$b_y = B\frac{\partial \xi_y}{\partial z}$$

$$b_z = -B\left(\frac{\partial \xi_x}{\partial x} + \frac{\partial \xi_y}{\partial y}\right)$$

ξ_x and ξ_y are plasma displacements in the x and y directions and b_z is the z component of the magnetic perturbation. B is the magnitude of the ambient magnetic field, B, and the Alfvén velocity, A, is a function of x only.

There are two standard approaches to identifying the normal modes of a system. In one approach, the time variable is Fourier transformed and the properties of the normal modes are obtained as the eigenfunctions and eigenvalues of a differential equation. In the other approach, an initial value is assumed, the time variable is Laplace transformed, and the initial value enters into the differential equation and makes it inhomogeneous. The normal modes can be inferred from the singularities of the associated Green's function. If the differential equation is not singular in the spatial range of interest, the two approaches give the same results. Since the first approach has the virtue of simplicity, it is frequently used to determine the normal modes of a system.

When the differential equation is singular, slowly decaying quasi-eigenmodes may be found in addition to the purely oscillatory normal modes. The solutions are usually not only singular but also multivalued. The multivaluedness can be removed by an appeal to causality. However, it is difficult to incorporate this requirement into the first approach. Since the second approach uses an initial value, causality is naturally built in. This approach provides a way of finding the quasi-eigenmodes more transparently, despite being mathematically more complicated.

Since the differential equation in this problem is singular, the Laplace transform technique is used to solve the problem. The homogeneity in y and z allows one to take their Fourier transforms. Without causing ambiguity, we use the same variables to denote the Fourier-Laplace transformed quantities.

The Laplace transform is calculated by multiplying the equations by $\exp(i\omega t)$ and integrating t from 0 to ∞. For the convergence of the transform, or equivalently for the requirement of causality, it is required that ω have a positive imaginary part. We therefore, specify that ω_i, the imaginary part of ω, must satisfy $\omega_i \geq \gamma > 0$. The coupled equations now read

$$\left(\frac{\omega^2}{A^2} - k^2\right)\xi_x = \frac{1}{B}\frac{db_z}{dx} - \frac{\dot{\xi}_x(0) - i\omega\xi_x(0)}{A^2}$$

$$\left(\frac{\omega^2}{A^2} - k^2\right)\xi_y = \frac{i\lambda b_z}{B} - \frac{\dot{\xi}_y(0) - i\omega\xi_y(0)}{A^2}$$

$$b_x = ikB\,\xi_x$$

$$b_y = ikB\,\xi_y \qquad (3)$$

$$b_z = -i\lambda B\,\xi_y - B\frac{\partial \xi_x}{\partial x}$$

where

$$\dot{\xi}_x(0) = \left[\frac{\partial \xi_x}{\partial t}\right]_{t=0} \qquad \dot{\xi}_y(0) = \left[\frac{\partial \xi_y}{\partial t}\right]_{t=0}$$

Here the Fourier transforms of y and z are equivalent to assuming that all variables have the same dependence on y and z: $e^{i(\lambda y + kz)}$. The variables ξ_x and ξ_y can be eliminated in terms of b_z and its derivatives so that

$$\frac{d}{dx}\left[\frac{1}{\frac{\omega^2}{A^2} - k^2}\frac{db_z}{dx}\right] + \frac{\frac{\omega^2}{A^2} - k^2 - \lambda^2}{\frac{\omega^2}{A^2} - k^2}\,b_z = b_o(x,\omega) \qquad (4)$$

where

$$b_o(x,\omega) = \frac{d}{dx}\left[\frac{B}{A^2}\frac{\dot{\xi}_x(0) - i\omega\xi_x(0)}{\frac{\omega^2}{A^2} - k^2}\right] + \frac{i\lambda B}{A^2}\frac{\dot{\xi}_y(0) - i\omega\xi_y(0)}{\frac{\omega^2}{A^2} - k^2}$$

denotes the initial perturbation. The boundary conditions for b_z are that at $x = a$ and $x = b$

$$\left[\frac{db_z}{dx}\right]_{x=a} = 0 \qquad \left[\frac{db_z}{dx}\right]_{x=b} = 0 \qquad (5)$$

Since (4) is not homogeneous, formally one can solve the above equation by first constructing the Green's function of the operator on the left-hand side of (4):

$$\frac{d}{dx}\left[\frac{1}{\frac{\omega^2}{A^2} - k^2}\frac{dG}{dx}\right] + \frac{\frac{\omega^2}{A^2} - k^2 - \lambda^2}{\frac{\omega^2}{A^2} - k^2}\,G = \delta(x - x') \qquad (6)$$

where $\delta(x)$ is the Dirac delta function, and then using Green's formula to express b_z in an integral form:

$$b_z(x,\omega) = \int_a^b G(x,x',\omega)b_o(x',\omega)dx' \qquad (7)$$

The inverse Laplace transform gives the time evolution of the perturbation:

$$b_z(x,t) = \frac{1}{2\pi}\int_F b_z(x,\omega)e^{-i\omega t}d\omega \qquad (8)$$

As noted above the requirement of causality imposes limitations on the integration path F. We choose it to run parallel to the real ω axis along $\omega_i \geq \gamma$.

The integration path F can be deformed to smaller ω_i as long as $G(x,x',\omega)$ remains analytic. The procedure for deformation is that adopted in the Landau damping problem and also used by bit Sedláček [1971]. The path is continuously deformed by decreasing ω_i until it

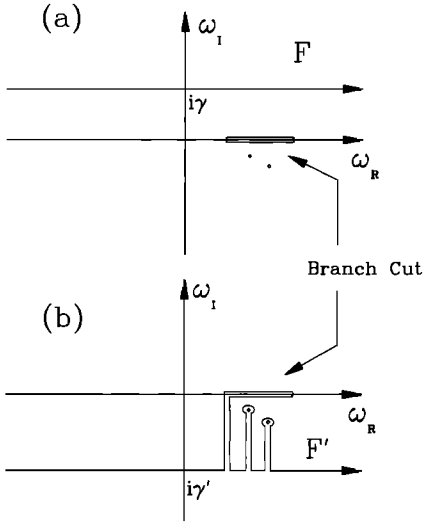

Fig. 1. (a) The complex ω plane with branch cut and singularities. The integration path F is defined to run above all of them at a sufficiently large value of γ to assure proper convergence. (b) The complex ω plane with a deformed integration path F'. Asymptotically, the integration along the branch cut and around the singularities will contribute the temporal variation.

meets the singularities or the branch cuts of the Green's function. Figure 1 shows schematically how the singularities and the branch cuts affect the deformation of the path. In this figure, it is assumed that the integrand has two isolated singularities and a continuum of singularities along the real ω axis and that the multivaluedness of the integrand has been removed by the branch cut extending from ω_a to ω_b. As the original integration path F is deformed to smaller ω_i, the branch cut line and singularities prevent the contour from "sliding by" and the contour is deformed as shown in Figure 1*b*. Because the contribution of the integration along other parts of F', the deformed F contour, is exponentially small, the temporal variation of the perturbation for large t can be obtained by asymptotic estimation of the integral around the singularities or branch cuts of the integrand. As we will see later, the contributions near the isolated singularities correspond to the collective oscillations while the contribution of the integration along the branch cut corresponds to the continuous spectrum [*Sedláček*, 1971]. Our interest is in the collective oscillations, so the isolated singularities of the integrand are of primary interest in this work.

The Green's Function of the Differential Equation

Although we will not use the Green's function formalism (for example, (8)) to obtain the perturbation fields, we will find it a powerful tool for understanding the properties of the solution and for identifying the frequency of the damped collective oscillations in a numerical solution. Thus, in this section we discuss the properties of the Green's function.

There exists a well-known theorem for constructing a Green's function from the solution of the homogeneous differential equation with the same operator [Friedman, 1956]. Suppose b_1 and b_2 are two linearly independent solutions of the homogeneous differential equation that satisfy the lower and upper boundary conditions, respectively:

$$\frac{d}{dx}\left[\frac{1}{\frac{\omega^2}{A^2}-k^2}\frac{db_1}{dx}\right]+\frac{\frac{\omega^2}{A^2}-k^2-\lambda^2}{\frac{\omega^2}{A^2}-k^2}b_1 = 0 \qquad \left[\frac{db_1}{dx}\right]_{x=a} = 0$$

$$\frac{d}{dx}\left[\frac{1}{\frac{\omega^2}{A^2}-k^2}\frac{db_2}{dx}\right]+\frac{\frac{\omega^2}{A^2}-k^2-\lambda^2}{\frac{\omega^2}{A^2}-k^2}b_2 = 0 \qquad \left[\frac{db_2}{dx}\right]_{x=b} = 0 \tag{9}$$

The Green's function for the differential equation can be expressed in terms of b_1 and b_2 as $G(x,x',\omega) =$

$$\frac{b_1(x)b_2(x')H(x'-x)+b_1(x')b_2(x)H(x-x')}{J} \tag{10}$$

where $H(x)$ is the Heaviside function:

$$H(x)=1 \quad x>0$$

$$H(x)=0 \quad x<0$$

and

$$J(\omega) = \frac{\frac{db_2}{dx}b_1-\frac{db_1}{dx}b_2}{\frac{\omega^2}{A^2}-k^2} \tag{11}$$

is called the conjunct (which is closely related to the Wronskian) of b_1 and b_2.

From the expression for G in (10), it is seen that $J=0$ corresponds to the singular points of G. From the discussion at the end of the last section and by making use of the theorem that J is not a function of x [Friedman, 1956], it is easy to see that the collective modes of the system correspond to the ω for which $J=0$.

For illustrative purposes, let us select a simple case by assuming that the Alfvén velocity varies as

$$A^2 \sim \frac{1}{x}$$

Because the multiplicative factor in A can always be absorbed into the definition of ω^2, the coefficient of the Alfvén velocity can be taken as unity. Equivalently, by assuming the coefficient to be unity, we have introduced a scaling factor to normalize the Alfvén velocity, or equivalently, the frequency.

With the Alfvén velocity specified, the Frobenius method can be used to obtain the series solution of b_z near the singularity of the differential equation. The singularity is located at

$$x_\omega = \frac{k^2}{\omega^2} = x_r + ix_i \tag{12}$$

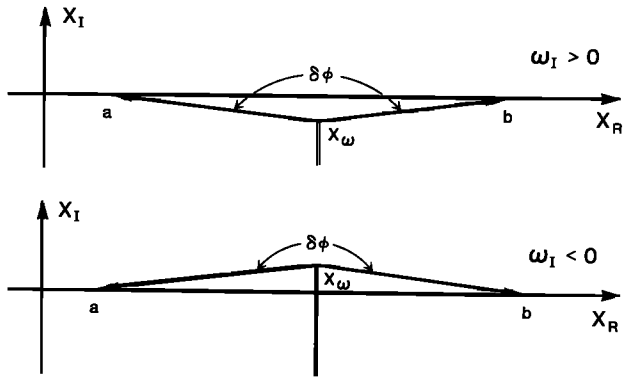

Fig. 2. The branch cut in the complex x plane for the case $\omega_r > 0$. In the upper panel, $\omega_i \geq \gamma > 0$. In the lower panel, $\gamma \leq \omega_i < 0$. With this branch cut, the change of the argument of $x - x_\omega$ when x varies from left of the branch cut to the right will be approximately π.

If $a < x_r < b$, b_z has one solution that is regular at the singularity and one that is not:

$$R(x) = (x - x_\omega)^2 + \frac{\lambda^2 (x - x_\omega)^4}{8} + \ldots$$
$$S(x) = \frac{\lambda^2 R(x) ln(x - x_\omega)}{2} + 1 - \frac{\omega^2 (x - x_\omega)^3}{3} + \ldots \quad (13)$$

Any solution of b_z can be constructed from a linear combination of the two solutions $R(x)$ and $S(x)$. Formally, one can use combinations of $R(x)$ and $S(x)$ to construct b_1 and b_2 that satisfy the lower and upper boundary conditions respectively; J can be related to $R(x)$ and $S(x)$ as

$$J(\omega) = C\left[S'(a)R'(b) - S'(b)R'(a)\right] \quad (14)$$

where C is a constant and

$$R'(x) = \frac{dR(x)}{dx} \qquad S'(x) = \frac{dS(x)}{dx}$$

Now, R and S are implicit functions of ω, and the ω that makes J zero must be that for which

$$\frac{S'(a)}{S'(b)} = \frac{R'(a)}{R'(b)} \quad (15)$$

Because the function $S(x)$ has a logarithmic term, it is a multivalued function. To make it single-valued, a branch cut must be made in the complex x plane (the branch cut here should not be confused with the branch cut in the frequency domain). The direction of the branch cut that extends from the singularity x_ω must be determined by the analytic properties of the Green's function. As we have already seen, the Green's function is analytic for any complex frequency with $\omega_i \geq \gamma > 0$. Because of (12), if k is real then

$$x_i = -\frac{2\omega_r \omega_i k^2}{|\omega|^4}$$

Clearly the singularities fall below x_i=0 if $\omega_r > 0$ and above x_i=0 when $\omega_r < 0$ (ω_r is the real part of ω) because of the requirement that $\omega_i \geq \gamma > 0$.

Let us for the moment consider the $\omega_r > 0$ case. The singularity is located in the lower half x plane as illustrated in the upper panel of Figure 2. When x varies along the real axis from $x = a$ to $x = b$, the change of argument of $x - x_\omega$, $\delta\phi$, is about $-\pi$. This property must be maintained as the contour of integration for ω is deformed to negative ω_i corresponding to the lower panel of Figure 2. Note that the singularity now appears at $x_i > 0$. By selecting a branch line that radiates parallel to the imaginary axis from the singularity $x = x_\omega$ to $-i\infty$, we guarantee that $\delta\phi \simeq -\pi$ remains valid. The branch cut for the $\omega_r < 0$ case can be worked out by the same principle. The purpose of the branch cut is to enforce the change of the argument of $x - x_\omega$ in a specific way so that the $\omega_i < 0$ case is the analytic continuation of the $\omega_i > 0$ case.

It is worthwhile to point out the differences between the analytic continuation done in Sedláček's work and in this work. After assuming a special density variation, Sedláček was able to solve the differential equation completely in an analytic form. He then did his analytic continuation in the frequency (ω) plane. The analytic continuation we have done is in the coordinate plane. The advantage of doing it in this way is that one no longer needs to solve the differential equation analytically for the whole spatial region before doing the analytic continuation. In most cases, it is impossible to obtain an analytic solution of a singular differential equation other than as an infinite series. In such circumstances, the method we outline here is useful since it requires an analytic expression only in the vicinity of the singularity of a differential equation.

As there are an infinite number of Riemann sheets for the logarithmic function in the solution $S(x)$, it may seem necessary to select a particular Riemann sheet for the analysis; fortunately, the results are unaffected by the choice of the Riemann sheet. From (13), it is seen that the singular solution, $S(x)$, on the nth Riemann sheet differs from the one in the principal Riemann sheet by $i\lambda^2 \pi n R(x)$. This term can be absorbed into the term in $R(x)$ in the expressions for b_1 and b_2 and cancels out in (15). The net effect is only to change the arbitrary constants of b_1 and b_2. This proves the uniqueness.

The temporal asymptotes of the perturbation can be obtained from the asymptotic estimation of the integrals along the branch cuts and around the singularity of the integrand in the ω integration. From (10) and (13), it follows that the Green's function $G(x, x', \omega)$ has eight logarithmic branch points on the real ω axis at

$$\pm kA(a) \quad \pm kA(x) \quad \pm kA(x') \quad \pm kA(b)$$

If the ω plane is cut as in Figure 3, the integrand becomes single valued in ω. Since the branch cut singular points are all located on the real ω axis, the integrations along the branch cut and around the branch cut singularities contribute time variations decaying as a negative power of time. The integration around the isolated singularity, located off the real ω axis and not illustrated, contributes an exponential decay in time.

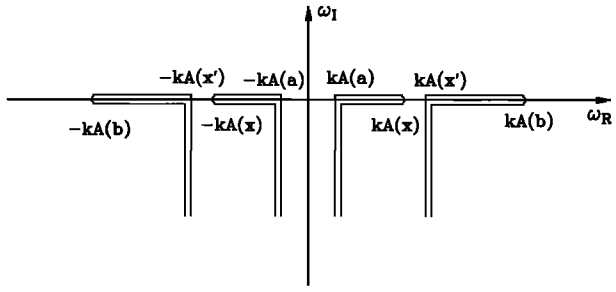

Fig. 3. The branch cuts that can make the integrand of (7) single valued. These branch cuts are very similar to those described by *Sedláček* [1971]. The isolated singularities of the Green's function are located somewhere in the lower half of the ω plane and are not shown in the plot.

These features of the solution have been qualitatively discussed by *Kivelson and Southwood* [1986]. Detailed mathematical discussions can also be found in the book by *Lighthill* [1958]. *Sedláček* [1971] solved a similar type of differential equation; the complex singularities discussed by Sedláček are of the same form as the singularities corresponding to the discrete solutions to our problem. Sedláček's analysis and discussion have great relevance to this work and the interested reader is referred to his work.

The Numerical Method

Although the basic physical features of the problem have been described in the previous sections, the singular nature of the differential equation poses difficulties in obtaining further analytical results since the solution cannot be expressed by standard functions. The functions $R(x)$ and $S(x)$ contain the unknown parameter ω and can only be used iteratively to determine the ω that makes J zero. Thus one turns to a numerical approach.

The numerical scheme adopted in this work can be outlined as follows. First a test frequency ω is selected; then the location of the singularity of the differential equation is determined for the test frequency ω. From the series solution (13), one can estimate the functions $R(x)$ and $S(x)$ and their derivatives near the singularity x_ω by using the leading terms in their Taylor expansion:

$$\begin{aligned} R(x) &\rightarrow (x-x_\omega)^2 \\ S(x) &\rightarrow 1. \\ R'(x) &\rightarrow 2(x-x_\omega) \\ S'(x) &\rightarrow \lambda^2(x-x_\omega)[\frac{1}{2}+ln(x-x_\omega)] \end{aligned} \tag{16}$$

If these expressions are used to represent the solution near $x = x_\omega$, the differential equation (9) is integrated numerically from the regions near x_ω to the lower and upper boundaries. Two pieces of solutions are obtained. One starts from the lower boundary to x_ω^{-0}. The other starts from x_ω^{+0} to the upper boundary. To connect these two pieces of solutions properly, one has to invoke the results we obtained from previous discussion on the analyticity of the Green's function which tells us how to select the right contour to round the logrithmic singularity of $S(x)$. Once this is done, boundary values $R'(a), R'(b), S'(a), S'(b)$ can be obtained. Using these values, the function J can be estimated from (14). By calculating J for several different values of ω, one can rapidly determine ω_n (n=1,2,3,...., the harmonic number), the root of J, with very good accuracy. Finally, the numerical integration of the differential equation is carried out for $\omega=\omega_n$ to obtain the wave phase and amplitude variation over x. The numerical method we used to integrate the differential equation was first suggested by *Budden* [1961]. Numerically, it is more appropriate to discuss the coupled differential equations in dimensionless form. Lengths can be normalized by $1/k$, and the magnetic perturbation can be normalized by the ambient magnetic field, B, corresponding to the replacements:

$$\begin{aligned} kx &\rightarrow x \\ k\xi_x &\rightarrow \xi_x \\ kA &\rightarrow A \\ b_z/B &\rightarrow b_z \end{aligned}$$

To solve the homogeneous equation (9), it is useful to rewrite it in the form

$$\begin{aligned} \frac{db_z}{dx} &= \left(\frac{\omega^2}{A^2}-1\right)\xi_x \\ \frac{d\xi_x}{dx} &= -\frac{\frac{\omega^2}{A^2}-1-\lambda^2}{\frac{\omega^2}{A^2}-1}b_z \end{aligned} \tag{17}$$

here ξ_x corresponds to the first term in brackets in (9) and b_z represents b_1 (b_2) which satisfies the lower (upper) boundary condition. If one starts the calculation sufficiently close to x_ω, one can use the first terms in (16) as the approximate initial value for b_z, and ξ_x there can be inferred from (17). Using the finite difference method, one can integrate the differential equations to the lower and upper boundaries.

A few free parameters are needed for the calculation. Throughout this work, we selected $a = 0.1$ and $b = 10$; λ was varied to determine the dependence of the damping of the collective mode on this parameter. It has been shown analytically that the collective mode is undamped if λ is zero or very large [*Dungey*, 1967]. Thus there must be at least one λ that causes the collective mode to be most heavily damped.

Numerical Results and Discussion

It is found from our numerical calculation that for any fixed λ, there are a few global collective modes with different complex frequencies. If the Green's functions for these modes are plotted with respect to x, it is observed that the larger the real part of the frequency, the greater the number of spatial nodes along the x axis. In Figure 4, we plot the amplitudes (the solid line) and relative phases (the dotted line) versus x for the magnetic field b_x, b_y and b_z perturbations for the first four modes with λ=0.5. The phase of each component is shown relative to fixed reference values at the lower bound-

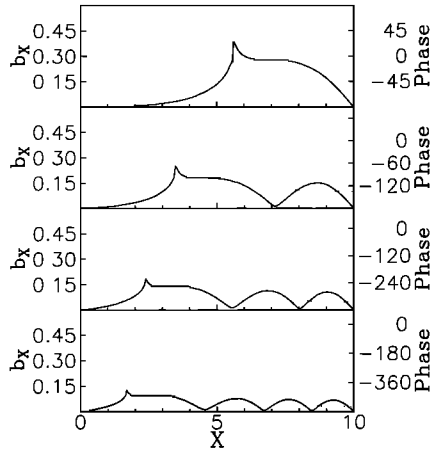

Fig. 4a The amplitudes (the solid lines) and the phases (the dotted lines) of the magnetic field perturbation in the x direction for λ=0.5. The corresponding harmonic number, real frequency and normalized damping rate (the ratio of the imaginary to the real part of the frequencies) are, from the top panel to the bottom panel: the first harmonic (n=1), $\omega_r = 0.42$, $\gamma = -0.012$; the second harmonic (n=2), $\omega_r = 0.54$, $\gamma = -0.011$; the third harmonic (n=3), $\omega_r = 0.65$, $\gamma = -0.010$; and the fourth harmonic (n=4), $\omega_r = 0.77$, $\gamma = -0.009$. Properties of the same four harmonics are shown in Figures 7 and 8 where the mode frequencies and damping rates are shown directly on the plots for the different panels. Note that λ is the normalized "azimuthal" wave number, i.e., the wave number in the y (azimuthal) direction divided by the wave number in the z (field-aligned) direction. In the amplitude plot, each harmonic has been normalized by taking the largest amplitude of either b_x, b_y or b_z to be unity. In the phase plot, the phase of each component relative to fixed reference values at the lower boundary of the box is plotted.

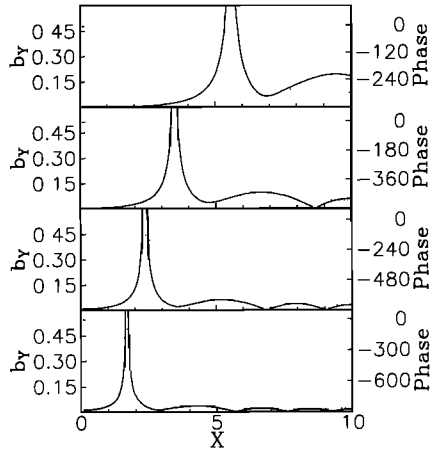

Fig. 4b As in Figure 4a for the magnetic field perturbation in the y direction.

ary of the box. From this figure one can see that although b_z varies smoothly throughout the box region, b_x changes abruptly and b_y becomes very large at the singular point. The behavior at the singularity varies among the harmonics. It should be emphasized that the plot shows the wave structure along the x axis at an intermediate time scale, i.e., at a time long enough to neglect the transient effects of the initial perturbation but short enough to be able to observe the exponentially damped modes. It is seen from Figure 4 that the fundamental mode has one node in the box for b_z and the higher harmonics have accordingly more nodes. One may note that the node of each component is not strictly zero, especially for the node close to the resonant field line. The appearance of such behavior is closely related to the finite damping of the mode. As the mode frequency becomes a complex value, the quasi-eigenfunction is also a complex function. The real part and the imaginary part of the function do not necessarily go to zero at the same position. In fact the zeros for the real part and the imaginary part of the function are offset by a small value. This small value should be proportional to γ, the ratio of the imaginary part of the mode frequency to the real part of it. This nonzero node behavior is very important for the mode to transport wave energy from the global mode to the resonant field line. If the wave amplitude turns out to be exactly zero, the Poynting vector, which is plotted in Figure 8, will vanish at those nodes and cannot transport the wave energy all the way to the resonant field line.

The numerical results obtained here can be compared with the results of *Allan et al.* [1986a]. Despite the different geometries used, similar global mode structures have been obtained (compare with Figure 6 of their paper). This similarity indicates that the appearances of the global modes are intrinsic properties of ULF waves in the inhomogeneous system and are not significantly modified by the curved field geometry they used. The details of the inhomogeneity, for example, whether it is caused by the nonuniformity of the magnetic field or plasma density or both of them, are expected to modify the solution in minor ways.

In their work, Allan et al. noticed that different harmonics have different damping rates. Since they assumed finite absorption by the ionosphere, the damping rates they calculated came from both wave mode coupling and ionospheric absorption and it is difficult to separate these two effects in their calculation. On the other hand, in our study, no ionospheric damping is in-

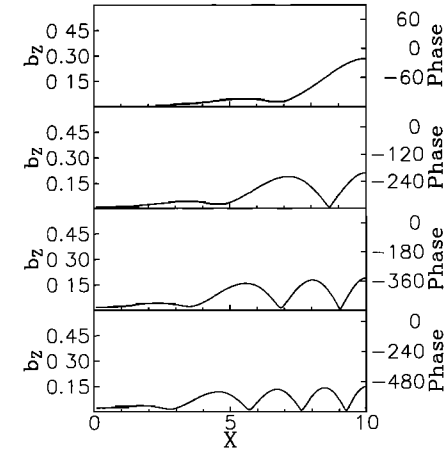

Fig. 4c As in Figure 4a for the magnetic field perturbation in the z direction.

TABLE 1. Numerical Results for the First Three Global Mode Harmonics

λ	ω_r	ω_i	ω_i/ω_r	$\lambda^2/\omega^{4/3}$
		First Harmonic		
0.06	4.15×10^{-1}	2.57×10^{-4}	6.19×10^{-4}	1.16×10^{-2}
0.10	4.16×10^{-1}	7.09×10^{-4}	1.71×10^{-3}	3.22×10^{-2}
0.20	4.17×10^{-1}	2.70×10^{-3}	6.47×10^{-3}	1.29×10^{-1}
0.30	4.17×10^{-1}	5.21×10^{-3}	1.25×10^{-2}	2.84×10^{-1}
0.40	4.19×10^{-1}	6.30×10^{-3}	1.51×10^{-2}	5.11×10^{-1}
0.50	4.23×10^{-1}	4.95×10^{-3}	1.17×10^{-2}	7.88×10^{-1}
0.60	4.31×10^{-1}	2.91×10^{-3}	6.75×10^{-3}	1.11
0.70	4.44×10^{-1}	1.43×10^{-3}	3.21×10^{-3}	1.45
0.80	4.60×10^{-1}	6.09×10^{-4}	1.33×10^{-3}	1.80
0.90	4.78×10^{-1}	2.33×10^{-4}	4.87×10^{-4}	2.17
1.00	4.99×10^{-1}	8.10×10^{-5}	1.62×10^{-4}	2.53
		Second Harmonic		
0.06	5.21×10^{-1}	1.97×10^{-4}	3.78×10^{-4}	8.58×10^{-3}
0.10	5.22×10^{-1}	5.44×10^{-4}	1.04×10^{-3}	2.38×10^{-2}
0.20	5.24×10^{-1}	2.08×10^{-3}	3.97×10^{-3}	9.48×10^{-2}
0.30	5.27×10^{-1}	4.20×10^{-3}	7.97×10^{-3}	2.13×10^{-1}
0.40	5.30×10^{-1}	5.86×10^{-3}	1.10×10^{-2}	3.73×10^{-1}
0.50	5.36×10^{-1}	5.84×10^{-3}	1.09×10^{-2}	5.74×10^{-1}
0.60	5.45×10^{-1}	4.41×10^{-3}	8.09×10^{-3}	8.09×10^{-1}
0.70	5.58×10^{-1}	2.77×10^{-3}	4.97×10^{-3}	1.07
0.80	5.74×10^{-1}	1.54×10^{-3}	2.69×10^{-3}	1.34
0.90	5.93×10^{-1}	7.89×10^{-4}	1.33×10^{-4}	1.63
1.00	6.14×10^{-1}	3.73×10^{-4}	6.07×10^{-4}	1.92
		Third Harmonic		
0.06	6.33×10^{-1}	1.72×10^{-4}	2.71×10^{-4}	6.62×10^{-3}
0.10	6.33×10^{-1}	4.74×10^{-4}	7.48×10^{-4}	1.84×10^{-2}
0.20	6.36×10^{-1}	1.83×10^{-3}	2.88×10^{-3}	7.32×10^{-2}
0.30	6.39×10^{-1}	3.80×10^{-3}	5.95×10^{-3}	1.63×10^{-1}
0.40	6.44×10^{-1}	5.74×10^{-3}	8.91×10^{-2}	2.88×10^{-1}
0.50	6.50×10^{-1}	6.61×10^{-3}	1.02×10^{-2}	4.44×10^{-1}
0.60	6.58×10^{-1}	5.95×10^{-3}	9.05×10^{-3}	6.29×10^{-1}
0.70	6.70×10^{-1}	4.43×10^{-3}	6.62×10^{-3}	8.37×10^{-1}
0.80	6.85×10^{-1}	2.91×10^{-3}	4.26×10^{-3}	1.06
0.90	7.02×10^{-1}	1.76×10^{-3}	2.50×10^{-3}	1.30
1.00	7.23×10^{-1}	9.89×10^{-4}	1.37×10^{-3}	1.54

cluded. Because the damping rate obtained here comes purely from the contribution of the mode coupling, one can study the parameter dependence of the damping rate on λ and other parameters.

Numerical results for the first three global mode harmonics corresponding to different assumed values of λ are summarized in Table 1. The first column from the left is λ, and the second and the third columns are the real and imaginary parts of the mode frequencies. The fourth column is the relative damping rate, i.e., the ratio of the imaginary part to the real part of the frequencies. The right-hand column lists a calculated parameter defined as $\lambda^2/\omega^{4/3}$ whose physical significance is discussed below.

From Table 1, one sees that for the same harmonic, both the real and the imaginary parts of the frequencies change with λ. However the imaginary part is much more sensitive to λ than is the real part; for example, for the first harmonic, the imaginary part changes by almost one order of magnitude between λ=0.1 and λ=0.4, while the change of the real part is less than 2%. This indicates that the compressional and shear Alfvén modes couple very strongly at certain azimuthal wave numbers λ.

In discussing how damping rate changes with λ, the work of *Forslund et al.* [1975] is pertinent. In an investigation of radio wave absorption by a plasma, Forslund et al. obtained numerical solutions of an equation (their equation (2)) that has a form similar to our equation (4) (note the finite temperature correction in their calculation has only minor effects). They discovered that the rate of absorption was largest for a specific angle of incidence of the radio wave. The absorption rate was found to be a function of the dimensionless quantity $\alpha = (k_0L)^{2/3}\sin^2\theta_0$; ($k_0$ is the wave number, L is characteristic scale of the inhomogeneity, and θ_0 is the incident angle of the radio wave). Figure 5 reproduces their results. By comparing the quantities in the two equations, we find that α, the dimensionless quantity plotted in Figure 5, is equivalent to $(\lambda^2/\omega^{4/3})[A(x_\omega)]^2/[A'(x_\omega)]^{2/3}$. For the Alfvén wave velocity used in this problem $[A(x_\omega)]^2/[A'(x_\omega)]^{2/3} = 2^{2/3}$, and this constant is unimportant for the analysis. In the right-hand column of Table 1, the ratio $\lambda^2/\omega^{4/3}$ is tabulated. This ratio is also referred as the coupling parameter by *Kivelson and Southwood* [1986]. Note that because Forslund et al. assumed a continuous source, they were interested in calculating the rate of absorption. In our work, there is no continuous source, so we calculate the temporal damping rate of the mode which corresponds to the rate of absorption of wave energy by excitations of the system. Indeed, the relative damping rate we calculate is of the same order of magnitude as the absorption rate found by Forslund et al.

Figure 6 shows the relative damping rates of the first three harmonics as functions of the coupling parameter. It is seen that the shape of the curves is similar to the Forslund et al. curve of Figure 5. One can also note that the maximum damping rates for the different harmonics occur for slightly different coupling parameters. Table 1 reveals that the maximum damping rate depends weakly on λ. Allan et al., whose parameter m corresponds to 10λ because of a different normalization,

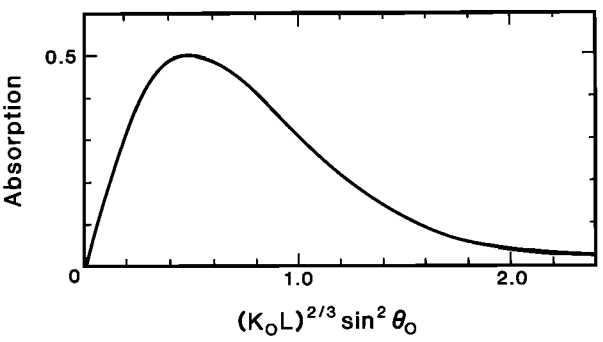

Fig. 5. The absorption rate of the plasma as a function of the coupling parameter indicated on the figure. The figure is reproduced from *Kivelson and Southwood* [1986].

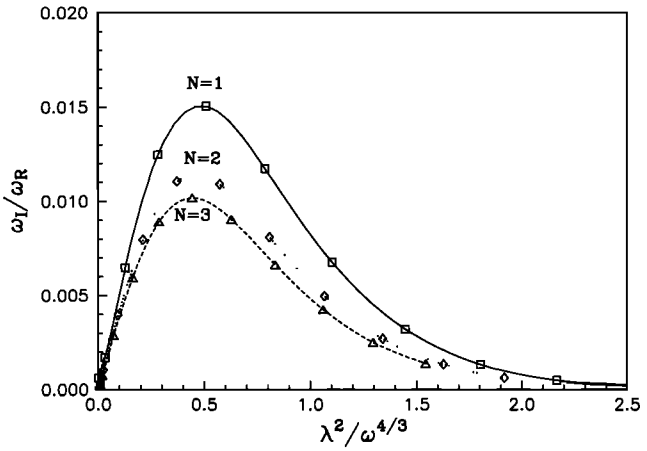

Fig. 6. The relative damping for first three harmonics of the global mode as a function of the coupling parameter. Note the similar functional behavior of the functions plotted in Figure 5 and Figure 6.

also noticed that for different harmonics the maximum coupling occurred at different m values. For the fundamental mode (their (1,1) resonance), Allan et al. found that the strongest coupling occurs at m=3, or equivalently λ=0.3. This is very close to our result as we find strongest coupling at λ=0.5. The small discrepancy may arise from the different geometry used in the two studies. For higher harmonics, Allan et al. found the strongest coupling shifted to larger m. Owing to the limitations of their numerical method, they found that it was very difficult to separate the different harmonics so that individual harmonics could be studied in detail. Parts of their conclusions concerning the higher harmonics may be spurious because of what they describe as contamination of data.

Additional properties of these global modes can be described by using our numerical results. For example, wave polarization as a function of position can be determined. In Figure 7, we have plotted the phase angle by which the b_y perturbation leads the b_x perturbation. When this phase angle is either positive or less than $-180°$, the wave is left hand polarized and when it is greater than $-180°$ but less than $0°$, the wave is right hand polarized. It is seen from this figure that the polarization reverses at x_ω, the resonant field line position. However, reversals also occur when $x \neq x_\omega$. The number of polarization reversals along the x axis increases with the harmonic order. Thus the polarization reversal alone should not be used to locate the resonant field line position in interpreting observed Pc 3–5 pulsation events as is frequently done.

There is another parameter that characterizes the resonant field line position very distinctly. This parameter is the Poynting vector which has been used to study energy flows of ULF waves in the terrestrial magnetosphere [*Junginger*, 1985; *Junginger et al.*, 1985]. Figure 8 plots the x (radial) component of the Poynting vector. Since the wave mode has finite damping, the Poynting vector is defined as

$$S(x) = \frac{\omega_r}{2\pi}\int_0^{\frac{2\pi}{\omega_r}} (Re(E) \times Re(b))\, dt$$

It is seen that the Poynting vector reverses sign only across the resonant field line, indicating that the energy flows to the resonant field line from both left and right sides. Since the field perturbation amplitude is evanescent on the left side of the resonant field line, it is easy to understand that the amplitude of the Poynting vector is smaller on the left than on the right side. The increase in magnitude of the Poynting vector near the resonant field line indicates that the energy of the global mode perturbation is extracted to excite the continuous spectrum of shear Alfvén oscillations most strongly near resonant field lines.

OBSERVATION EVIDENCE FOR GLOBAL MODES

The global mode model was proposed as an explanation of certain firmly established qualitative features of Pc 3–5 waves in the terrestrial magnetosphere. Examples include the occasional excitation of nearly monochromatic signals independent of latitude (or L shell) and reported observations of very small azimuthal wave number events (see *Kivelson and Southwood*, [1986] for a discussion). Quantitative tests are only now being initiated.

One suggestive study is that of *Crowley et al.* [1987]. Using the European incoherent scatter radar (EISCAT) and ground-based magnetometer measurements, Crowley et al. studied two large-amplitude Pc 5 pulsations excited by a sudden impulse. The ionospheric electron density, inferred for the northern hemisphere from EISCAT measurements and modeled for the southern hemisphere ionosphere, predicted a higher damping rate of the pulsation than was observed. The authors suggested that the ionospheric damping might have been competing with wave growth controlled by the global mode of the magnetosphere. Once the global mode is excited, it continuously feeds energy at a known rate into the field

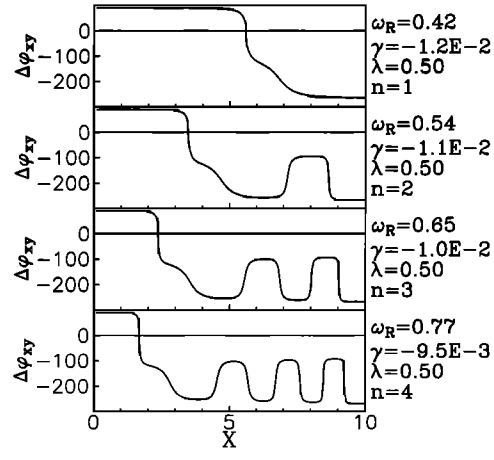

Fig. 7. The phase by which the magnetic perturbation b_y leads b_x for each harmonic plotted in Figure 4. When the phase crosses zero and $-180°$, the polarization reverses. Plotted at the side of each panel are the corresponding global mode frequency, relative damping rate, λ and harmonic number n. Note λ is the normalized "azimuthal" wave number, i.e., the wave number in the y (azimuthal) direction divided by the wave number in the z (field-aligned) direction.

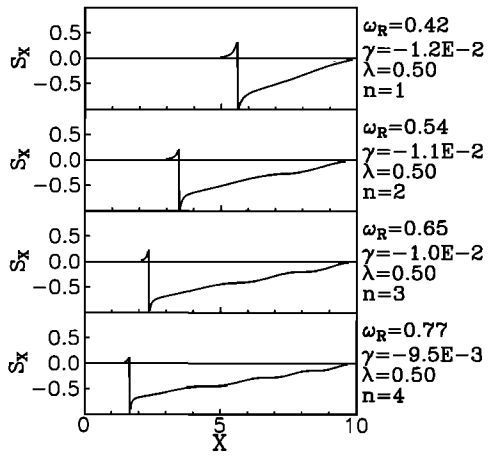

Fig. 8. The x component of the Poynting vector for each harmonic plotted in Figure 4. The only change of sign of the Poynting vector occurs at the resonant field line location and the increase of magnitude toward the resonant field line indicates that global mode energy flows toward the resonant field line from both directions.

line through the Poynting vector we discussed above. Crowley et al. found that the rate required in their case was of the order predicted from the global mode calculations.

Other aspects of the global mode predictions remain to be tested. For example, the predicted amplitude and phase structure described in this work should be relevant to compressional perturbations observed on radial passes through the dayside magnetosphere. However, the unique features of the spatial structure will be clear only if the small-amplitude perturbations far from the resonant field line can be identified.

Summary and Conclusion

In an inhomogeneous magnetized plasma, the compressional Alfvén wave mode is coupled to the shear Alfvén wave mode. Because of this wave mode coupling, MHD waves in an inhomogeneous magnetized plasma differ substantially from waves present in the homogeneous case. For homogeneous magnetized plasmas, the compressional Alfvén wave and the shear Alfvén wave can exist independently so that any perturbation can be decomposed into these two wave modes. The inhomogeneity of either magnetic field or plasma density distribution, which may be characterized by the variation of the Alfvén velocity through space, couples these two wave modes. Perturbations in the inhomogeneous magnetized plasma can no longer be separated into the compressional Alfvén mode and the shear Alfvén mode. Rather the perturbation has characteristics of both wave modes. One interesting feature which emerges in the inhomogeneous case is that the perturbation may behave quite differently on different time scales. Immediately following the disappearance of the transients, the perturbation is characterized by components of collective oscillations, i.e., oscillations with same frequency over the whole spatial region. The collective oscillation damps exponentially, and at long times the perturbation is characterized by the oscillations of all field lines with their own resonant frequencies in both radial and azimuthal directions. The component in the radial direction damps as a negative power of time. In a nondissipative system for the long time limit, perturbations are characterized by each field line oscillating with its own resonant frequency purely in the azimuthal direction.

The major features of the above points have been discussed qualitatively by *Kivelson and Southwood* [1985, 1986]. In this work we have confirmed them quantitatively. In addition, through the Laplace transform approach and the Green's function formalism, we have presented a way to formulate the coupled ULF wave problem for further analytical discussions. The numerical results reveal the spatial profiles of the wave modes and other associated wave properties.

Concerning the possible application of our results to data analysis, we emphasize that two distinct observational features, namely perturbations in which all field lines resonate at their natural frequencies and perturbation dominated by a single (global mode) frequency over a large part of the magnetosphere, may be present at times following an initial perturbation. The discrete frequency response should be observed only at times short enough so that the exponentially damped mode is still dominant. The former, namely the perturbations of field lines resonating at their natural frequencies, should be observed at times long enough to neglect the exponentially damped modes; and the commonly observed azimuthal polarization is consistent with the theoretical prediction that such polarization remains at very long times.

Properties of observed magnetospheric ULF pulsations that result from warm plasma effects, finite Larmor radius effects, or aspects of a realistic magnetic geometry such as particle trapping are beyond the scope of this work. Nonetheless, we believe that many magnetospheric observations can be interpreted on the basis of the model we have investigated.

Acknowledgments. The authors are grateful for the enlightening and helpful discussions and comments with D. J. Southwood, R. J. Walker and L. Chen and for the encouragement of W. Allan. One of us, X. M. Zhu is also grateful to Zhengkang Shen and Weinan E for their comments. This work was supported by the Division of Atmospheric Sciences of the National Science Foundation under grants ATM 83-00523 and ATM 86-10858. Institute of Geophysics and Planetary Physics Publication No 2911.

The Editor thanks two referees for their assistance in evaluating this paper.

References

Allan, W., S. P. White, and E. M. Poulter, Magnetospheric coupling of hydromagnetic waves–Initial results, *Geophys. Res. Lett.*, *12*, 287, 1985.

Allan, W., S. P. White, and E. M. Poulter, Impulse-excited hydromagnetic cavity and field-line resonances in the magnetosphere, *Planet. Space Sci.*, *34*, 371, 1986*a*.

Allan, W., S. P. White, and E. M. Poulter, Hydromagnetic wave coupling in the magnetosphere—plasmapause effects on impulse-excited resonances, *Planet. Space Sci.*, *34*, 1189, 1986*b*.

Appert, K., J. Vaclavik, and L. Villard, An introduction to the theory of Alfvén wave heating (with a sideglance of ICRF), lectures presented at Univ. Fed. Flumihense, Niteroi, Brasil, 1984.

Budden, K. G., *Radio Waves in the Ionosphere*, Cambridge University Press, New York, 1961.

Chen, L., and A. Hasegawa, A theory of long-period magnetic pulsations, 1, Steady state excitation of field line resonances, *J. Geophys. Res.*, *79*, 1024, 1974*a*.

Chen, L., and A. Hasegawa, A theory of long-period magnetic pulsations, 2, Impulse excitations of surface eigenmode, *J. Geophys. Res.*, *79*, 1033, 1974*b*.

Crowley, G., W. J. Hughes, and T. B. Jones, Observational evidence of cavity modes in the Earth's magnetosphere, *J. Geophys. Res.*, *92*, 12233, 1987.

Cummings, W. D., R. J. O'Sullivan, and P. J. Coleman,Jr., Standing Alfvén waves in the magnetosphere, *J. Geophys. Res.*, *74*, 778, 1969.

Dungey, J. W., *Hydromagnetic Waves*, in *Physics of Geomagnetic Phenomena*, edited by S. Matsushita and W. H. Campbell, pp.913-934, Academic, New York, 1967.

Engebretson, M. J., L. J. Zanetti, and T. A. Potemra, Harmonically structured ULF pulsations observed by the AMPTE CCE magnetic field experiment, *Geophys. Res. Lett.*, *13*, 405, 1986.

Forslund, D., J. M. Kindel, K. Lee, E. L. Lindman, and R. L. Morse, Theory and simulation of absorption in a hot plasma, *Phys. Rev. A*, *11*, 679, 1975.

Friedman, B., *Principles and Techniques of Applied Mathematics*, John Wiley, New York, 1956.

Greenstadt, E. W., R. L. McPherron, R. R. Amderson, and F. L. Scarf, A storm time, Pc 5 event observed in the outer magnetosphere by ISEE 1 and 2: Wave properties, *J. Geophys. Res.*, *91*, 13398, 1986.

Inhester, B., Numerical modeling of hydromagnetic wave coupling in the magnetosphere, *J. Geophys. Res.*, *92*, 4751, 1987.

Jacobs, J. A., T. Kato, S. Matsushita, and V. A. Troitskaya, Classification of geomagnetic micropulsations, *J. Geophys. Res.*, *69*, 180, 1964.

Junginger, H., Poynting vector as a diagnostic of hydromagnetic wave structure, *J. Geophys. Res.*, *90*, 4155, 1985.

Junginger, H., G. Haerendel, and F. Melsner, A statistical study of wave Poynting vectors measured during long-period magnetospheric pulsations at geostationary orbit, *J. Geophys. Res.*, *90*, 8301, 1985.

Kivelson, M. G., and D. J. Southwood, Resonant ULF waves: A new interpretation, *Geophys. Res. Lett.*, *12*, 49, 1985.

Kivelson, M. G., and D. J. Southwood, Coupling of global magnetospheric MHD eigenmodes to field line resonances, *J. Geophys. Res.*, *91*, 4345, 1986.

Kivelson, M. G. , J. Etcheto, and J. G. Trotignon, Global compressional oscillations of the terrestrial magnetosphere: The evidence and a model, *J. Geophys. Res.*, *89*, 9851, 1984.

Lighthill, M. J., *Introduction to Fourier Analysis and Generalised Functions*, Cambridge University Press, New York, 1958.

Lin, C. C., *The Theory of Hydrodynamic Stability*, Cambridge University Press, New York, 1955.

Piliya, A. D., Wave conversion in an inhomogeneous plasma, *Sov. Phys. Tech. Phys.*, Engl. Transl., *11*, 609, 1966.

Radoski, H. R., A note on the problem of hydromagnetic resonances in the magnetosphere, *Planet. Space Sci.*, *19*, 1012, 1971.

Samson, J. C., Three-dimensional polarisation characteristics of high- latitude Pc 5 geomagnetic micropulsations, *J. Geophys. Res.*, *77*, 6145, 1972.

Sedláček, Z. , Electrostatic oscillations in a cold inhomogeneous plasma, 1, Differential equation approach, *J. Plasma Phys.*, *5*, 239, 1971.

Southwood, D. J., Some features of field line resonance in the magnetosphere, *Planet. Space Sci.*, *22*, 483, 1974.

Southwood, D. J., Comments on field line resonances and micropulsations, *Geophys. J. R. Astron. Soc.*, *41*, 425, 1975.

Southwood, D. J., and W. J. Hughes, Theory of hydromagnetic waves in the magnetosphere, *Space Sci. Rev.*, *35*, 301, 1983.

Takahashi, K., and R. L. McPherron, Harmonic structure of Pc 3–4 pulsations, *J. Geophys. Res.*, *87*, 1054, 1982.

White, R. B., and F. F. Chen, Amplification and absorption of electromagnetic waves in overdense plasma, *Plasma Phys.*, *16*, 565, 1974.

M. G. Kivelson and X. Zhu, Department of Earth and Space Scieneces and Institute of Geophysics and Planetary Physics, University of California at Los Angeles, CA 90024 -1567.

(Received January 27, 1987;
revised April 18, 1988;
accepted April 18, 1988.)